
Claudin-4 SPECT Imaging Allows Detection of Aplastic Lesions in a Mouse Model of Breast Cancer

Michael Mosley¹, James Knight¹, Albrecht Neesse², Patrick Michl³, Manuela Iezzi⁴, Veerle Kersemans¹, and Bart Cornelissen¹

¹CR-UK/MRC Gray Institute for Radiation Oncology and Biology, University of Oxford, Oxford, United Kingdom; ²Department of Gastroenterology II, University Medical Center, Georg-August University, Göttingen, Germany; ³Department of Gastroenterology, Endocrinology, Infectiology and Metabolism, Philipps University Marburg, Marburg, Germany; and ⁴Department of Medicine and Aging Sciences, G. d'Annunzio University of Chieti-Pescara, Chieti, Italy

The expression of claudin-4, a protein involved in tight junction complexes, is widely dysregulated in epithelial malignancies. Claudin-4 is overexpressed in several premalignant precursor lesions, including those of cancers of the breast, pancreas, and prostate, and is associated with poor survival. A noncytotoxic C-terminal fragment of *Clostridium perfringens* enterotoxin (cCPE) is a natural ligand for claudin-4. Here, we demonstrate whole-body quantitative SPECT imaging of preneoplastic breast cancer tissue using ¹¹¹In-labeled cCPE. **Methods:** cCPE.GST or GST (GST is glutathione S-transferase) was conjugated to the metal ion chelator benzyl-diethylenetriaminepentaacetic acid to allow ¹¹¹In radiolabeling. The affinity of radiolabeled cCPE.GST for claudin-4 was confirmed using claudin-4-expressing MDA-MB-468 and SQ20b cells, compared with claudin-4-negative HT1080 cells. In vivo SPECT imaging was performed using athymic mice bearing MDA-MB-468 or HT1080 xenografts and using genetically modified BALB/*neuT* mice, which spontaneously develop claudin-4-expressing breast cancer lesions. **Results:** The uptake of ¹¹¹In-cCPE.GST in claudin-4-positive MDA-MB-468 xenograft tumors in athymic mice was significantly higher than in ¹¹¹In-GST or claudin-4-negative HT1080 tumors (6.72 ± 0.18 vs. 3.88 ± 1.00 vs. 2.36 ± 1.25 percentage injected dose per gram [%ID/g]; $P < 0.0001$). No other significant differences were observed in any of the examined organs. BALB/*neuT* mice, expressing rat *neuT* under *mmtv* promoter control, spontaneously developed tumorous lesions within their mammary fat pads over the course of 130 d. Overt mammary tumors were claudin-4-positive, and ¹¹¹In-cCPE.GST uptake was 3.2 ± 0.70 %ID/g, significantly higher than ¹¹¹In-GST (1.00 ± 0.60 %ID/g; $P < 0.05$). Mammary fat pads in mice aged 80 d bore claudin-4-positive aplastic lesions and accumulated ¹¹¹In-cCPE.GST (3.17 ± 0.51 %ID/g) but not ¹¹¹In-GST (0.99 ± 0.39 %ID/g; $P < 0.001$). **Conclusion:** Taken together, ¹¹¹In-cCPE.GST targets claudin-4 expression in frank tumors and preneoplastic tissue, and cCPE imaging may be used as an early detection tool for breast, prostate, and pancreatic cancer.

Key Words: claudin-4; cCPE; SPECT; tumorigenesis; breast cancer

J Nucl Med 2015; 56:745–751

DOI: 10.2967/jnumed.114.152496

The early detection of cancer greatly increases the chances for successful treatment and long-term survival, and early diagnosis of cancer by medical imaging is certainly the major contributor to a reduction in mortality for breast cancer over the last decade (<http://www.who.int>) (1). Even though the ability to detect precancerous lesions would further improve the facility for early intervention and improved patient outcome, to date, few effective imaging methods exist to detect precancerous lesions. Here, we propose that molecular imaging using SPECT of the increased expression of claudin-4 in precancerous lesions of the breast has the potential to improve early detection.

Claudin-4 is a 22-kDa member of the 27-member claudin protein family and is a vital component in adherens and tight junction complexes (2), which are widely dysregulated in epithelial malignancies (3). Claudin-4 expression can be used to distinguish certain types of cancers (4), since it is overexpressed in several premalignant precursor lesions compared with normal tissue, including lesions in the pancreas (5), prostate (6), lung (7), colon (8), and breast (3,9,10), for which claudin-4 overexpression is associated with poor prognosis. The exact mechanistic role of claudin-4 during tumorigenesis, and its role in solid tumors, remains to be elucidated (3). Nevertheless, it can act as a valid clinical biomarker for early diagnosis, as laid out in a recent review by Kwon et al. on ovarian cancers (3). Also, Neesse et al. explored the possibility of claudin-4 targeting using fluorescently labeled proteins as imaging biomarkers in pancreatic cancer (5).

Imaging of claudin-4 has been shown by Neesse et al. to be an effective way to detect precancerous lesions of the pancreas (5). *Clostridium perfringens* enterotoxin (CPE), which causes the symptoms of a common food poisoning, is a natural ligand for claudin-4 (11). It is a single polypeptide of approximately 35 kDa in size and is associated with type A food poisoning and such non-food-borne gastrointestinal diseases as antibiotic-associated diarrhea and sporadic diarrhea (12). The CPE receptor-binding activity of full-length CPE (319 aa) is restricted to the 30 C-terminal amino acids (13). Recently, site-directed mutagenesis revealed 3 Tyr residues, located at positions 306, 310, and 312, to be critical for receptor

Received Dec. 5, 2014; revision accepted Feb. 16, 2015.

For correspondence or reprints contact: Bart Cornelissen, CR-UK/MRC Oxford Institute for Radiation Oncology, Department of Oncology, University of Oxford, Old Rd. Campus Research Building, Off Roosevelt Dr., Oxford OX3 7LJ, U.K.

E-mail: bart.cornelissen@oncology.ox.ac.uk

Published online Apr. 3, 2015.

COPYRIGHT © 2015 by the Society of Nuclear Medicine and Molecular Imaging, Inc.

binding to claudin-4. Furthermore, competitive binding experiments showed that C-terminal CPE (cCPE, residues 184–319, 15 kDa) binds with 1:1 stoichiometry and submicromolar affinity to pure claudin-4. It has been shown that cCPE is sufficient to bind claudin-4 but does not exert cytotoxicity because it lacks residues 80–106 necessary for membrane insertion and pore formation (14).

Nesse et al. used a Cy5.5-labeled glutathione S-transferase (GST)-tagged version of cCPE (cCPE.GST, 41 kDa) and showed excellent uptake in claudin-4-expressing xenografts as well as in claudin-4-expressing pancreatic tumors in an engineered mouse model of KRAS mutation-induced pancreatic ductal adenocarcinoma. Earlier, Cocco et al. showed similar results using a fluorescein isothiocyanate-conjugated cCPE in models of ovarian cancer (15). However, the direct clinical translation of optical imaging approaches is limited by penetration depth of light, which is less than a couple of millimeters. To overcome this obstacle, we have now labeled cCPE with the radionuclide ^{111}In , which emits tissue-penetrating γ rays that can be detected by noninvasive SPECT imaging.

Here, we present our results on ^{111}In -labeled cCPE.GST. We demonstrate the possibility of whole-body, noninvasive imaging of claudin-4 expression in 2 models of breast cancer in mice. We further establish the possibility of early detection of precancerous aplastic lesions in a mouse model of human epidermal growth factor receptor-2 (HER2)-overexpressing breast adenocarcinoma.

MATERIALS AND METHODS

A COOH-terminal fragment of CPE (aa 184–319) linked to a GST fusion protein has previously been produced by Patrick Michl (5). Purity was confirmed by sodium dodecyl sulfate polyacrylamide gel electrophoresis (Supplemental Fig. 1; supplemental materials are available at <http://jnm.snmjournals.org>). A detailed procedure is laid out in the supplemental data. Purified cCPE.GST or GST was conjugated to benzyl-diethylenetriaminepentaacetic acid to allow radiolabeling with ^{111}In , as previously described (16). A detailed procedure is laid out in the supplemental data.

MDA-MB-468, SQ20b, and HT1080 human cancer cells were obtained from the American Type Culture Collection. Cells were tested and authenticated by the provider, using short tandem repeat profiling. The length of time in culture of these cells was less than 6 mo after retrieval from liquid nitrogen storage. Cells were cultured in 5% CO_2 in Dulbecco modified Eagle cell culture medium (Sigma-Aldrich) supplemented with 10% fetal calf serum (Invitrogen) and penicillin/streptomycin (100 units/mL; Invitrogen).

Aliquots of 2×10^5 MDA-MB-468, SQ20b, or HT1080 cells were seeded on coverslips and allowed to adhere overnight. To determine claudin-4 expression, and the ability of cCPE to bind, cells were washed twice with phosphate-buffered saline; fixed for 10 min at room temperature with 4% paraformaldehyde (Sigma); blocked with 2% bovine serum albumin in phosphate-buffered saline (pH 7.4) for 1 h; incubated with mouse anti-claudin-4 antibodies (clone 382321 [R&D Systems]; 1:400 dilution in blocking buffer) for 1 h at 37°C and, after 3 washes, goat antimouse antibody (1:250 dilution; Invitrogen) labeled with AlexaFluor594 for 1 h at 37°C; and mounted using Vectashield containing 2-(4-amidinophenyl)-1H-indole-6-carboxamide (DAPI) (Vector Laboratories). Confocal images were acquired using a Zeiss 530 confocal microscope (Zeiss). Results were confirmed using Western blot on whole cell lysates derived from all 3 cell lines, staining with anti-claudin-4 antibodies.

To investigate the binding of ^{111}In -cCPE.GST to claudin-4 receptors, aliquots of 2×10^5 MDA-MB-468, SQ20b, or HT1080 cells growing in a 24-well plate in 500 μL of growth medium were exposed

to 1–1,000 nM ^{111}In -cCPE.GST or ^{111}In -GST (1 MBq/ μg). After incubation for 1 h at 4°C, supernatant was removed and cells were washed and lysed using 0.1 M NaOH. Cell-associated and unbound ^{111}In were measured using an automated γ counter (Wizard²; Perkin Elmer). To determine intracellular fate after receptor binding, cells were exposed to 500 nM ^{111}In -cCPE.GST or ^{111}In -GST. At selected times, supernatant was removed from the cells, and cells were washed with 0.1 M glycine.HCl, pH 2.5, to remove cell surface-bound radioactivity and lysed using 0.1 M NaOH, as previously described (17). Radioactivity in cytoplasmic and nuclear fractions was counted in a γ counter. Binding affinity and the number of accessible binding sites were estimated by nonlinear regression analysis with a 1-site-total binding model using the software package GraphPad Prism (GraphPad Software Inc.). To study binding specificity, in some cases increasing amounts of cold, unlabeled cCPE.GST was added, to compete with the binding of 2 nM ^{111}In -cCPE.GST. The concentration at which half of the binding was prevented by the blocking agent (IC₅₀) values were calculated by nonlinear regression with a 1-site competition model with variable Hill slope using GraphPad Prism.

In Vivo Studies

All animal procedures were performed in accordance with the U.K. Animals (Scientific Procedures) Act 1986 and with local ethical committee approval. MDA-MB-468 or HT1080 xenografts were established in female athymic BALB/c *nu/nu* mice (Harlan). ^{111}In -cCPE.GST or ^{111}In -GST (5 MBq, 5 μg) was injected intravenously, and SPECT and CT images were acquired using a nanoSPECT-CT scanner (Bioscan) at 3 and 24 h after injection. Volume-of-interest analysis on SPECT images was performed using the Inveon Research Workplace software package (Siemens). After imaging, mice were sacrificed and selected tissues were removed, rinsed, blot dried, weighed. The amount of ^{111}In in each tissue was measured using an automated γ counter. Uptake was expressed as the percentage injected dose per gram of tissue (%ID/g).

The ability of ^{111}In -cCPE.GST to target claudin-4 in vivo was further studied in the BALB/*neuT* genetically engineered mouse model of breast cancer (18). A more detailed description of this mouse model is presented in the “Supplemental Methods” section. ^{111}In -cCPE.GST or GST imaging was performed as described above in BALB/*neuT* mice aged around 80 d, bearing aplastic lesions, or aged 120–140 d, bearing overt mammary tumors.

After imaging, sections (10 μm) were generated from snap-frozen tumor tissue harvested from xenografts and BALB/*neuT* mice. Sections were stained with hematoxylin and eosin to confirm histologic status. Other sections were stained for claudin-4, using mouse anti-claudin-4 antibodies (clone 382321; R&D systems), and mounted using Vectashield containing DAPI to stain for nuclei. Images were acquired using confocal microscopy as described above.

Statistical Analyses

All statistical analyses and nonlinear regression were performed using GraphPad Prism. 1 or 2-way ANOVA was used for multiple comparisons, with Tukey posttests to calculate significance of differences between groups. All data were obtained in triplicate or more independent replicates. Results are reported and graphed as average \pm SD, unless stated otherwise.

RESULTS

Reaction of a 4-fold excess of pSCN-Bn-diethylenetriaminepentaacetic acid (DTPA) with cCPE.GST or GST resulted in a conjugation yield of approximately 1 DTPA molecule per cCPE.GST or GST protein. ^{111}In radiolabeling yield, as determined by instant thin-layer chromatography or G25 size-exclusion

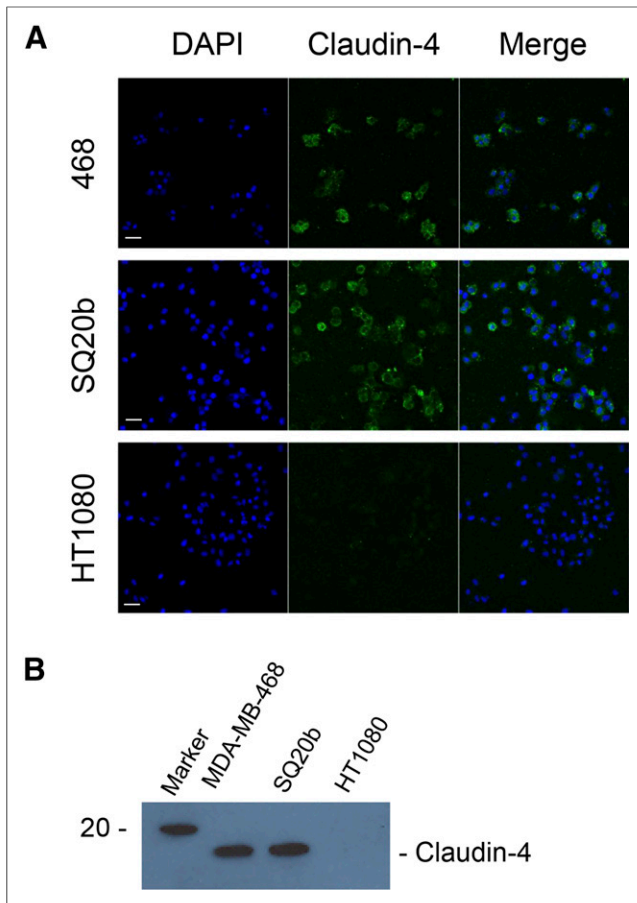


FIGURE 1. (A) MDA-MB-468, SQ20b, and HT1080 cells were stained for claudin-4. Scale bar, 20 μ m. (B) Western blot demonstrating presence or absence of claudin-4 in whole cell lysates obtained from MDA-MB-468, SQ20b, and HT1080 cells.

chromatography, was routinely greater than 95% (Supplemental Fig. 2).

The expression of claudin-4 on MDA-MB-468 and SQ20b cells, but not on HT1080 cells, was confirmed by immunocytochemistry and Western blot on whole cell lysates (Fig. 1). Densitometry further corroborated these results (Supplemental Figs. 3A and 3B). Relative claudin-4 signal on immunofluorescence images was significantly higher for MDA-MB-468 and SQ20b cells than HT1080 cells (3.74 ± 0.62 , 4.24 ± 0.51 , and 1.00 ± 0.11 , respectively; $P < 0.001$). Western blot signal showed a 22.2-fold- and a 22.8-fold-higher expression of claudin in MDA-MB-468 and SQ20b cells, respectively, than in HT1080.

The affinity of radiolabeled cCPE-GST for claudin-4 was confirmed by binding to claudin-4-expressing MDA-MB-468 and SQ20b cells but not to claudin-4-negative HT1080 cells (Fig. 2). After exposure of cells to ^{111}In -cCPE.GST, radioactivity associated with MDA-MB-468 cells was 24.1 ± 0.9 times higher for ^{111}In -cCPE.GST than ^{111}In -GST ($P < 0.001$). The association of ^{111}In -cCPE.GST was 4.7 ± 0.2 times higher with MDA-MB-468 than HT1080 cells ($P < 0.001$). The affinity of ^{111}In -cCPE.GST for claudin-4 receptors of $1.93 \pm 0.59 \mu\text{M}$ (K_D ; $R^2 = 0.99$) was comparable to earlier values of $0.65 \mu\text{M}$ for unmodified CPE binding to purified His₁₀-claudin-4 binding reported by Van Itallie et al. (14). It was calculated that each

MDA-MB-468 cell accommodates on average 3.9 ± 0.1 million copies of ^{111}In -cCPE.GST to its extracellular surface (maximum binding [B_{max}]). Blocking the specific binding of cCPE.GST to its receptor by addition of increasing amounts of cold, unlabeled cCPE.GST showed excellent specificity ($\text{Log}[IC_{50}] = 1.3 \pm 0.07 \text{ nM}$; $R^2 = 0.98$) (Fig. 2B).

The internalization analysis in MDA-MB-468, SQ20b, or HT1080 cells revealed that ^{111}In -cCPE.GST, but not ^{111}In -GST, was internalized in claudin-4-positive MDA-MB-468 and SQ20b cells but not in claudin-4-negative HT1080 cells (Supplemental Fig. 4A). The amount of ^{111}In internalized into SQ20b cells was markedly higher than into MDA-MB-468 cells (after 2 h, $0.61\% \pm 0.03\%$ of the added ^{111}In was found inside the cells, compared with $0.23\% \pm 0.04\%$ for MDA-MB-468 cells; $P < 0.0001$), even though the amount of ^{111}In -cCPE.GST associated with the membrane of either cell was not significantly different ($1.03\% \pm 0.17\%$ vs. $0.23\% \pm 0.11\%$, respectively; $P > 0.05$) (Supplemental Figs. 4A and 4B).

SPECT/CT imaging of athymic BALB/c mice carrying subcutaneous xenograft tumors revealed marked uptake of ^{111}In -cCPE.GST in MDA-MB-468 xenografts, but ^{111}In -GST uptake in MDA-MB-468 xenografts was significantly lower (6.72 ± 0.18 vs. $3.88 \pm 1.00 \text{ \%ID/g}$; $P < 0.0001$). ^{111}In -cCPE.GST was taken up in HT1080 tumors at much reduced levels ($2.36 \pm 1.25 \text{ \%ID/g}$; $P < 0.0001$) (Fig. 3A). Immunohistochemistry on sections obtained from tumor tissue showed claudin-4 overexpression in MDA-MB-468, but not in HT1080 xenografts (Fig. 3B), with densitometry corroborating these results (Supplemental Fig. 3C). Relative claudin-4 signal was 8.2 ± 1.5 -fold higher in MDA-MB-468 xenografts than HT1080 tumors ($P < 0.0001$). SPECT imaging results

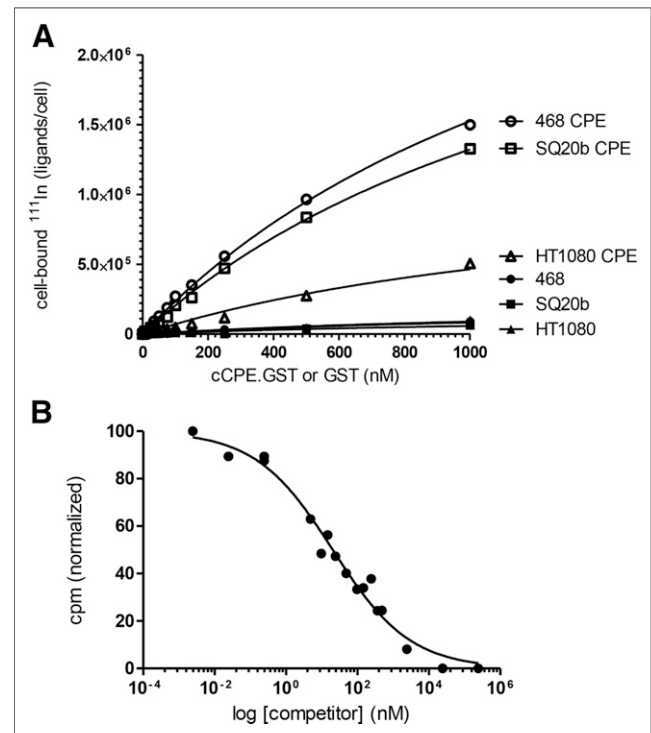


FIGURE 2. (A) MDA-MB-468 cells were exposed for 1 h at 4°C to increasing concentrations of ^{111}In -labeled cCPE.GST or GST, and extent of cell-binding was determined. (B) Increasing amounts of unlabeled cCPE.GST were used to block binding of ^{111}In -cCPE.GST to MDA-MB-468 cells.

were confirmed by γ counting of tumor tissues after dissection. ^{111}In -cCPE.GST uptake in MDA-MB-468 xenografts was 6.72 ± 0.18 %ID/g at 24 h after injection, significantly higher than ^{111}In -GST (3.88 ± 1.00 %ID/g; $P < 0.0001$) and uptake of ^{111}In -cCPE.GST in claudin-4-negative HT1080 xenografts (2.36 ± 1.16 %ID/g; $P < 0.0001$) (Fig. 3C). Uptake in normal tissues was limited, resulting in tumor-to-muscle and tumor-to-blood ratios of 7.83 ± 0.21 and 4.00 ± 0.11 , respectively, in MDA-MB-468 xenograft-bearing mice, 24 h after injection of ^{111}In -cCPE.GST, significantly higher than ^{111}In -GST or ^{111}In -cCPE.GST in HT1080 xenograft-bearing mice (tumor-to-muscle ratios, 4.53 ± 1.17 and 2.98 ± 1.57 , and tumor-to-blood ratios, 2.11 ± 0.54 and 1.32 ± 0.70 , respectively; $P < 0.05$; Fig. 3C). Uptake of ^{111}In was also observed in knee and shoulder joints, potentially a result from the use of DTPA as a chelator. Some limited uptake of ^{111}In -

cCPE.GST was observed in the intestines, especially the small intestine. It was also observed that uptake of ^{111}In -cCPE.GST in normal mammary fat pads in these animals was low (1.36 ± 0.35 %ID/g).

Claudin-4 expression in established mammary tumors, harvested from 120- to 140-d-old BALB/*neuT* mice, was confirmed using immunohistochemistry (Fig. 4A; Supplemental Fig. 4D). Claudin-4 signal from carcinomas was 3.1 ± 0.7 -fold higher than from normal muscle tissue. Histologic stage was confirmed using hematoxylin and eosin and anti-smooth muscle antigen staining (Supplemental Figs. 5A and 5B). Established tumors, measuring 280 mm^3 on average, were clearly visualized with ^{111}In -cCPE.GST on SPECT/CT images (Fig. 4B). Moreover, CT imaging could also visualize these tumors. Uptake of ^{111}In -cCPE.GST in tumor tissue in BALB/*neuT* mice was significantly higher than ^{111}In -GST control (at 3 h after injection, uptake was 8.50 ± 1.40 vs. 4.50 ± 1.10 %ID/g, respectively; $P < 0.01$) (Supplemental Fig. 6A). Muscle uptake was limited to less than 2 % ID/g (Supplemental Fig. 6B), leading to tumor-to-muscle ratios of 5.30 ± 2.10 and 1.30 ± 1.20 for ^{111}In -cCPE.GST and ^{111}In -GST, respectively, at 24 h after injection ($P < 0.05$) (Fig. 4C). Normal-tissue distribution was similar to that in athymic BALB/*c* mice (Supplemental Fig. 6C). No significant differences were observed between ^{111}In -cCPE.GST and GST in any of the tissues studied ($P > 0.05$).

Aplastic lesions, harvested from the mammary fat pads of BALB/*neuT* mice aged 80 d, showed increased levels of claudin-4, compared with low-level expression in breast muscle (3.3 ± 0.2 -fold higher; $P < 0.001$) and normal mammary fat pads (2.3 ± 0.1 -fold higher; $P < 0.001$), harvested from wild-type BALB/*c* mice (Fig. 5A; Supplemental Fig. 3E). Histologic stage was confirmed using hematoxylin and eosin staining (Supplemental Fig. 5). Representative SPECT/CT images are shown in Figure 5B. Moreover, these lesions accumulated ^{111}In -cCPE.GST (3.17 ± 0.51 %ID/g) but not ^{111}In -GST (0.99 ± 0.39 %ID/g; $P < 0.001$) (Fig. 5C). Notably, at this age, CT imaging did not reveal the presence of neoplastic tissue in any of the 6 mice studied.

DISCUSSION

Tumor-specific noninvasive molecular imaging tools have the possibility to revolutionize cancer detection, by allowing diagnosis at early stages of oncogenesis. Early diagnosis of any cancer type significantly improves the chances for survival. Although screening of the general population for all types of cancer with a single general technique is not economically feasible, the focused follow-up of high-risk patients may lead to markedly improved

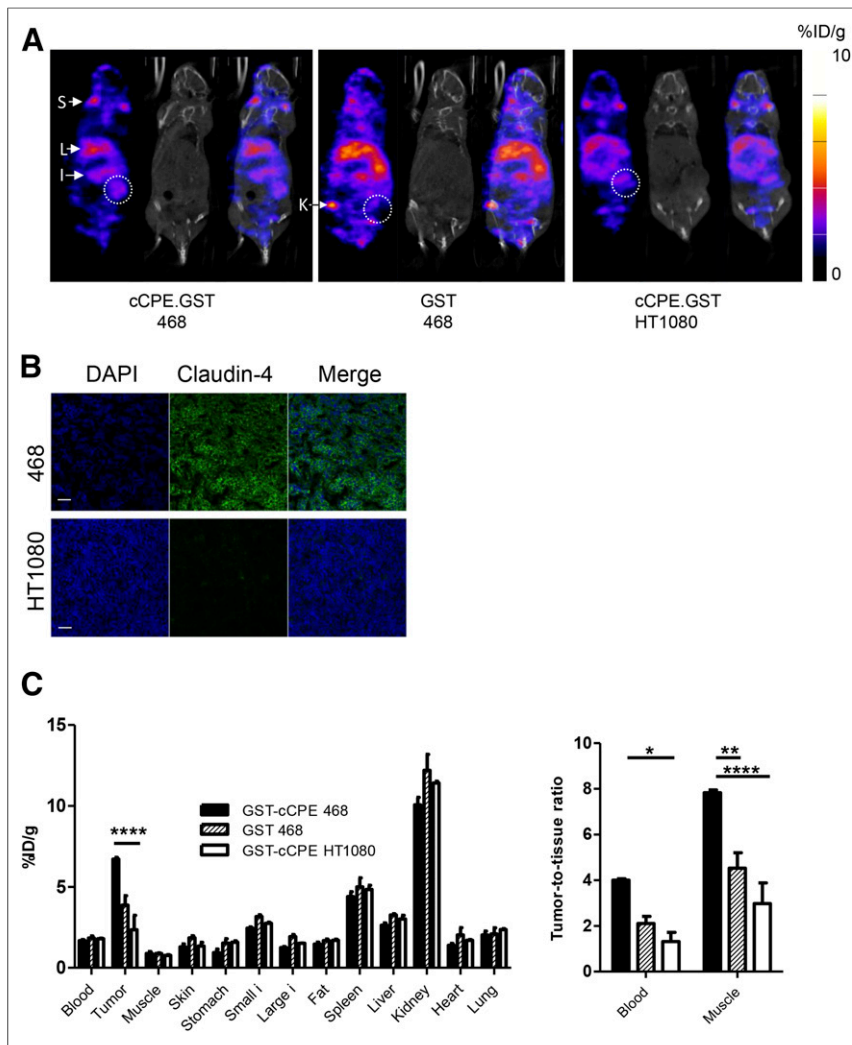


FIGURE 3. (A) Representative SPECT/CT images of mice carrying tumor xenografts (white circles) of MDA-MB-468 (claudin-4-positive) or HT1080 (claudin-4-negative) cells, 24 h after intravenous administration of ^{111}In -cCPE.GST or ^{111}In -GST. ^{111}In uptake was also observed in shoulder joints (S), liver (L), intestines (I), and knee joints (K). Coronal sections through tumor are shown. (B) Sections obtained from MDA-MB-468 or HT1080 xenograft tumors were stained using anticlaudin-4 antibodies. Scale bar, 20 μm . (C) Biodistribution results, 24 h after intravenous administration of ^{111}In -cCPE.GST or ^{111}In -GST. Tumor-to-blood and tumor-to-muscle ratios were calculated. Each group contained at least 3 animals. * $P < 0.05$. ** $P < 0.01$. *** $P < 0.001$. **** $P < 0.0001$.

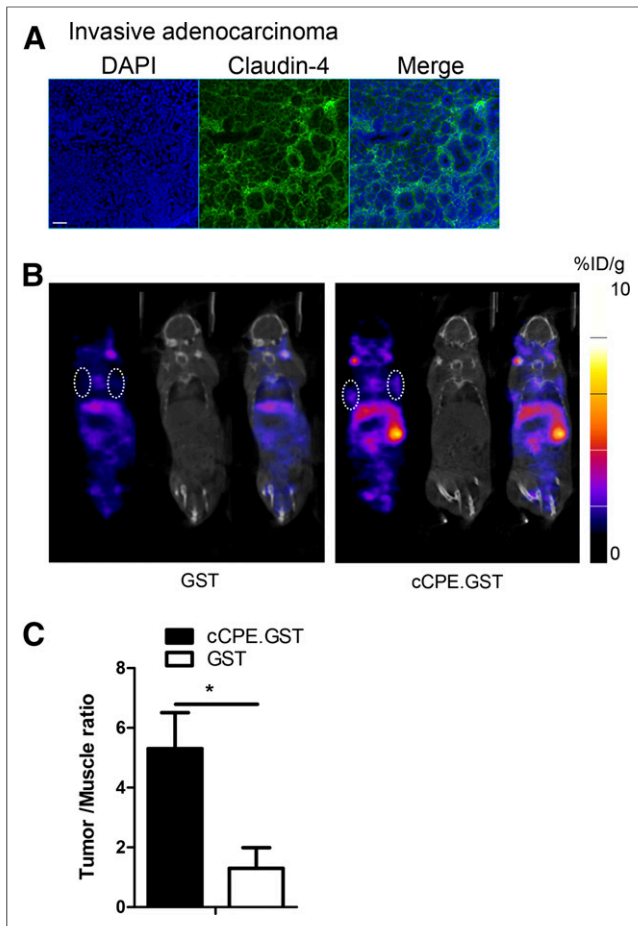


FIGURE 4. (A) Sections obtained from tumors harvested from 139-d-old BALB/*neuT* mouse were stained using anti-claudin-4 antibodies. Scale bar, 20 μ m. (B) Representative SPECT/CT images of BALB/*neuT* mice, aged 139 d, bearing mammary tumors (white circles), 24 h after intravenous administration of ^{111}In -cCPE.GST or ^{111}In -GST. Overt tumors were clearly visible on CT images. Coronal sections through tumor are shown. (C) Volume-of-interest analysis of BALB/*neuT* mice bearing overt tumors 3 or 24 h after injection of ^{111}In -cCPE.GST or ^{111}In -GST. Each group contained at least 3 animals. * $P < 0.05$.

survival in these groups. Examples of readily identifiable risk groups include those with germ-line mutations such as BRCA1 and 2, increasing the lifetime risk of breast and ovarian cancer (19), or those with hereditary risks of pancreatic cancer (20).

Neesse et al. showed that a fluorescently labeled fragment of the naturally occurring bacterial protein, CPE, fused to GST, was able to target pancreatic cancer in several mouse models (5). Importantly, it was demonstrated that imaging of Pan-In precursor lesions was possible. However, although fluorescence tomography imaging allowed visualization of claudin-4-expressing pancreatic tumors in KPC mice, this optical imaging method does not allow imaging of deep-seated lesions in human patients, given the limited penetration of infrared light. Nuclear medicine techniques can overcome this issue and allow easy translation from preclinical to human use.

Here we demonstrate, for the first time to our knowledge, that a radiolabeled version of the same fusion protein, cCPE.GST, allows noninvasive imaging of claudin-4-positive tumors in 2 mouse models of breast cancer. As a proof of principle, ^{111}In -cCPE.GST uptake

was evaluated in a subcutaneous tumor xenograft model and shown to target claudin-4. Because claudin-4 is well known as the CPE receptor causing gastroenteritis in the intestinal tract, some limited uptake of ^{111}In -cCPE.GST was observed in the intestines, especially the small intestine (5).

Previously, Foss et al. described the use of ^{125}I -labeled anti-claudin-4 whole IgG antibodies to target claudin-4 on Colo-357 and PANC-1 xenografts in mice (21), resulting in tumor-to-muscle uptake ratios of 4.3 and 6.3, respectively. However, these values were obtained at 4 and 6 d after administration of the labeled antibody, which is undesirable for clinical translation. Cy5.5-cCPE.GST signal in claudin-4-positive CAPAN-1 xenografts was approximately 2-fold higher than in claudin-4-negative HT1080 xenografts. Our results using the MDA-MB-468 xenograft model yielded average tumor-to-muscle ratios of 8:1 and a 3-fold-higher uptake than HT1080 tumors, reached at 24 h after injection. These results are positive, especially in light of a relatively unfavorable K_D . We hypothesized that the main factor influencing the high tumor uptake of ^{111}In -cCPE.GST may be the high number of cCPE receptors, calculated as 3.9 ± 0.1 million per cell. To aid clinical translation, optimization of the binding affinity to claudin-4 may be necessary, for example, through biochemical modification.

Given the well-known disadvantages associated with xenograft models (these disadvantages are reviewed in great detail elsewhere (22)), we set out to validate ^{111}In -cCPE.GST SPECT imaging in a genetically engineered mouse model of breast cancer, because these more faithfully represent human disease (18). Because cancer progression in BALB/*neuT* mice mimics that of HER2-positive ductal carcinoma in situ, the use of this spontaneous cancer model allowed us to study claudin-4 imaging during tumorigenesis. Our imaging results in BALB/*neuT* animals revealed tumor-to-muscle ratios of 4.8:1, even at 3 h after injection. Even though absolute tumor uptake levels decreased from 8.50 ± 1.40 to 3.20 ± 0.70 %ID/g at 24 h after injection, tumor-to-muscle increased to 5.3:1. Tumor uptake levels in BALB/*neuT* mice were lower than the xenograft studies but nevertheless reflect the expression of the target epitope, claudin-4, on the tumor versus normal tissues such as normal fat pad tissue or breast muscle tissue (Fig. 5).

Overt tumors in BALB/*neuT* mice were clearly visible on CT images. On the contrary, aplastic lesions, by their very nature, were too small to be detected using anatomic CT imaging. Because claudin-4 expression is upregulated at this early stage of tumor progression, ^{111}In -cCPE SPECT imaging allowed good visualization of preneoplastic lesions, at least in this tumor model. Given that tumors in this mouse model are palpable only on average when mice reach approximate ages of 130 d (18), SPECT imaging allows detection almost 40% (50 d) earlier, in mice aged 80 d, and before CT imaging. Given that x-ray imaging is currently used as the preferred method of breast cancer screening, our method of very-early detection may enable even earlier therapeutic intervention or trigger more frequent follow-up of patients at risk. Here, we have described a SPECT imaging method for claudin-4 imaging, but because PET imaging has a much increased sensitivity compared with SPECT, and PET results can be more easily quantified, a translation of the SPECT imaging method described here to PET imaging using alternative radioisotopes such as ^{89}Zr or ^{64}Cu would facilitate clinical translation. A limitation for clinical translation may be the potential immunoreactivity of cCPE. Currently, little information is available on the humoral response of humans to *C. perfringens*

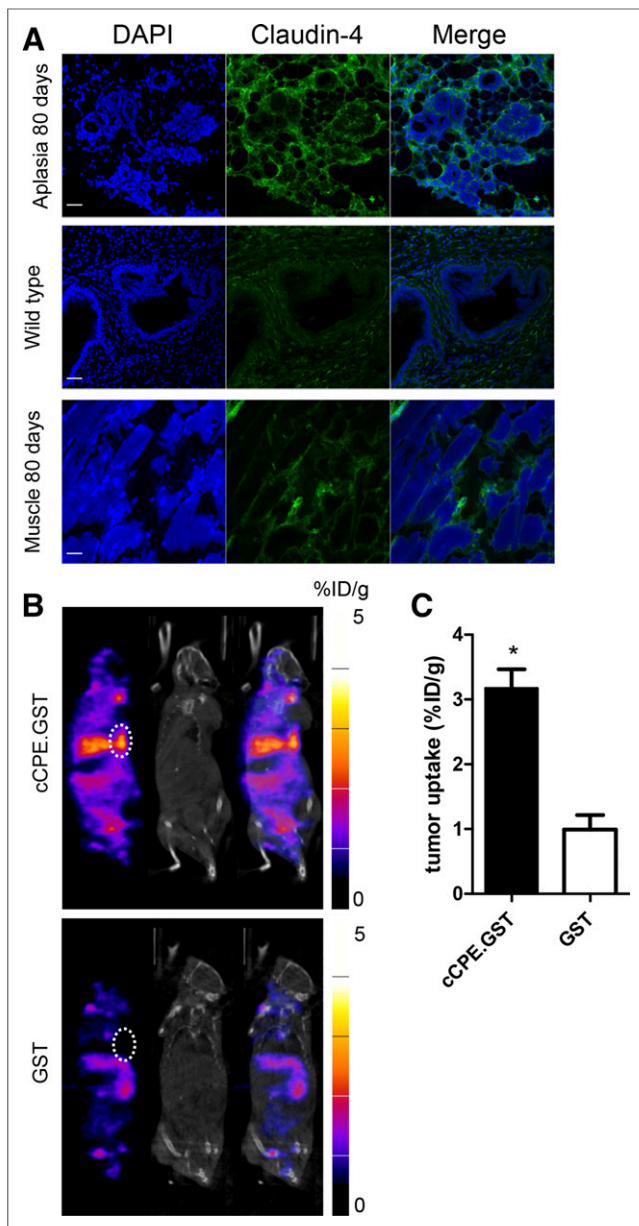


FIGURE 5. (A) Sections obtained from aplastic lesion or muscle harvested from 80-d-old BALB/*neuT* mouse or ductal tissue obtained from a wild-type BALB/*c* mouse were stained using anti-claudin-4 antibodies. Scale bar, 20 μ m. (B) Representative SPECT/CT images of BALB/*neuT* mice, aged 80 d, bearing aplastic lesions (white circles), 24 h after intravenous administration of ^{111}In -cCPE.GST or ^{111}In -GST. Functional SPECT imaging was compared with anatomic CT imaging. Aplanic lesion could not be detected on CT images. Coronal sections through mammary fat pads are shown. (C) Volume-of-interest analysis of 80-d-old BALB/*neuT* mice bearing aplastic 24 h after injection of ^{111}In -cCPE.GST or ^{111}In -GST. Each group contained at least 3 animals. * $P < 0.05$.

A toxins and the prevalence of preformed antibodies in the general population (23). Although we and others did not observe any adverse reactions in mice after repeated cCPE dosing (24), the safety and antigenicity of cCPE must be evaluated for future clinical application, especially in individuals with a history of *C. perfringens*-induced enteritis or after repeated exposure to cCPE as immune reactions due to preformed antibodies cannot be ruled out completely.

Claudins in general and claudin-4 in particular have a known involvement in epithelial-to-mesenchymal transition (EMT), the complex stepwise phenomenon that occurs during both embryonic development and very-early during tumorigenesis (25). A recent link between EMT and cancer stem cells has sparked considerable interest, because it is widely accepted that only a minor population of tumor cells can initiate and support the development of tumors, and the highly aggressive tumor cells share many characteristics of embryonic progenitor cells. Given that the crucial proteins snail, slug, and E-cadherin are involved in claudin regulation, it is tempting to link claudin-4-targeted imaging to the early detection of EMT. However, the limited amount of available evidence warrants further investigation to formally validate this association. Compared with other well-studied biomarkers, such as HER2, progesterone receptor, and estrogen receptor in breast cancer, claudin-4 (and -3) is less well understood, and the mechanisms that drive the intricate correlation between claudins and tumor progression remain a topic of intense research. Therefore, a better understanding of the role of claudins in tumorigenesis, tumor progression, EMT, and cancer stem cells may provide important information to elucidate the molecular mechanisms that underpin the use of claudins as imaging biomarkers and aid in the design of new imaging agents or multimodal imaging biomarkers (3).

Taken together, ^{111}In -labeled cCPE.GST is an improved agent for the imaging of claudin-4-positive tumorous lesions. Possible applications might include its use as an imaging biomarker for early detection cancer and preneoplasms, with applications in screening of breast, ovarian, lung, and pancreatic cancer (3). Previously reported data also demonstrate that claudin-4 positivity is retained in metastases, at least in the KPC murine pancreatic cancer model (5), and claudin-4 SPECT or PET imaging may be useful as a follow-up procedure to detect recurrent disease after curative therapies.

CONCLUSION

^{111}In -cCPE.GST targets claudin-4 expression in frank tumors and preneoplastic tissue in BALB/*neuT* mice. cCPE imaging may be used as an early detection tool for cancer of the breast, prostate, or pancreas.

DISCLOSURE

The costs of publication of this article were defrayed in part by the payment of page charges. Therefore, and solely to indicate this fact, this article is hereby marked "advertisement" in accordance with 18 USC section 1734. This research was supported by Cancer Research UK, the CR-UK/EPSCRC Cancer Imaging Centre in Oxford, and a Max Eder fellowship from the Deutsche Krebshilfe. No other potential conflict of interest relevant to this article was reported.

ACKNOWLEDGMENT

We thank Prof. Yasuhiko Horiguti at Osaka University for his support.

REFERENCES

1. Fass L. Imaging and cancer: a review. *Mol Oncol*. 2008;2:115–152.
2. Neesse A, Griesmann H, Gress TM, Michl P. Claudin-4 as therapeutic target in cancer. *Arch Biochem Biophys*. 2012;524:64–70.
3. Kwon MJ. Emerging roles of claudins in human cancer. *Int J Mol Sci*. 2013;14:18148–18180.

4. Kulka J, Szasz AM, Nemeth Z, et al. Expression of tight junction protein claudin-4 in basal-like breast carcinomas. *Pathol Oncol Res.* 2009;15:59–64.
5. Neesse A, Hahnenkamp A, Griesmann H, et al. Claudin-4-targeted optical imaging detects pancreatic cancer and its precursor lesions. *Gut.* 2013;62:1034–1043.
6. Landers KA, Samaratunga H, Teng L, et al. Identification of claudin-4 as a marker highly overexpressed in both primary and metastatic prostate cancer. *Br J Cancer.* 2008;99:491–501.
7. Shang X, Lin X, Alvarez E, Manorek G, Howell SB. Tight junction proteins claudin-3 and claudin-4 control tumor growth and metastases. *Neoplasia.* 2012;14:974–985.
8. Ersoz S, Mungan S, Cobanoglu U, Turgutalp H, Ozoran Y. Prognostic importance of claudin-1 and claudin-4 expression in colon carcinomas. *Pathol Res Pract.* 2011;207:285–289.
9. Kominsky SL, Vali M, Korz D, et al. Clostridium perfringens enterotoxin elicits rapid and specific cytolysis of breast carcinoma cells mediated through tight junction proteins claudin 3 and 4. *Am J Pathol.* 2004;164:1627–1633.
10. Lanigan F, McKiernan E, Brennan DJ, et al. Increased claudin-4 expression is associated with poor prognosis and high tumour grade in breast cancer. *Int J Cancer.* 2009;124:2088–2097.
11. Michl P, Buchholz M, Rolke M, et al. Claudin-4: a new target for pancreatic cancer treatment using clostridium perfringens enterotoxin. *Gastroenterology.* 2001;121:678–684.
12. Robertson SL, McClane BA. Interactions between clostridium perfringens enterotoxin and claudins. *Methods Mol Biol.* 2011;762:63–75.
13. Hanna PC, Wnek AP, McClane BA. Molecular cloning of the 3' half of the clostridium perfringens enterotoxin gene and demonstration that this region encodes receptor-binding activity. *J Bacteriol.* 1989;171:6815–6820.
14. Van Itallie CM, Betts L, Smedley JG 3rd, McClane BA, Anderson JM. Structure of the claudin-binding domain of clostridium perfringens enterotoxin. *J Biol Chem.* 2008;283:268–274.
15. Cocco E, Casagrande F, Bellone S, et al. Clostridium perfringens enterotoxin carboxy-terminal fragment is a novel tumor-homing peptide for human ovarian cancer. *BMC Cancer.* 2010;10:349–359.
16. Hnatowich DJ, Layne WW, Childs RL. The preparation and labeling of DTPA-coupled albumin. *Int J Appl Radiat Isot.* 1982;33:327–332.
17. Cornelissen B, Hu M, McLarty K, Costantini D, Reilly RM. Cellular penetration and nuclear importation properties of ¹¹¹In-labeled and ¹²⁵I-labeled HIV-1 tat peptide immunoconjugates in BT-474 human breast cancer cells. *Nucl Med Biol.* 2007;34:37–46.
18. Quaglino E, Mastini C, Forni G, Cavallo F. ErbB2 transgenic mice: a tool for investigation of the immune prevention and treatment of mammary carcinomas. *Curr Protoc Immunol.* 2008;Chapter 20:Unit 20 29 21–20 29–10.
19. Antoniou A, Pharoah PD, Narod S, et al. Average risks of breast and ovarian cancer associated with BRCA1 or BRCA2 mutations detected in case series unselected for family history: a combined analysis of 22 studies. *Am J Hum Genet.* 2003;72:1117–1130.
20. Klein AP, Hruban RH, Brune KA, Petersen GM, Goggins M. Familial pancreatic cancer. *Cancer J.* 2001;7:266–273.
21. Foss CA, Fox JJ, Feldmann G, et al. Radiolabeled anti-claudin 4 and anti-prostate stem cell antigen: initial imaging in experimental models of pancreatic cancer. *Mol Imaging.* 2007;6:131–139.
22. Richmond A, Su Y. Mouse xenograft models vs GEM models for human cancer therapeutics. *Dis Model Mech.* 2008;1:78–82.
23. Zarén E, Schwan A, Frenckner B. Age related variations of serum concentrations of normally occurring IgG antibodies to Clostridium perfringens. *J Clin Pathol.* 1987;40:282–285.
24. Suzuki H, Kondoh M, Li X, et al. A toxicological evaluation of a claudin modulator, the C-terminal fragment of clostridium perfringens enterotoxin, in mice. *Pharmazie.* 2011;66:543–546.
25. Wang Y, Zhou BP. Epithelial-mesenchymal transition in breast cancer progression and metastasis. *Chin J Cancer.* 2011;30:603–611.